

Rigorous Analysis of Chua's Circuit with a Smooth Nonlinearity

Zbigniew Galias, *Senior Member, IEEE,*

Abstract—Dynamics of Chua's circuit with a smooth nonlinearity is studied by means of interval arithmetic methods. We analyze behaviors of the system for several parameter values in the periodic and chaotic regions. For parameter values in the chaotic region, we find lower bounds for the topological entropy of a corresponding return map and prove that the system is chaotic in the topological sense. We find low-period orbits embedded in chaotic attractors and estimate the true value of the topological entropy. We construct a trapping region enclosing the spiral attractor and discuss how to prove the existence of a trapping region for the case of the double-scroll attractor.

Index Terms—chaos, topological entropy, Chua's circuit

I. INTRODUCTION

THE Chua's circuit is a simple electronic circuit exhibiting complex oscillatory dynamics [1], [2]. Dynamical behaviors and the problem of existence of chaos in this system has been studied extensively since the invention of the circuit [3], [4], [5], [6].

Most of the results presented in the literature are based on simulations of the circuit and analysis of geometrical models of observed attractors. The first rigorous result concerning the existence of chaos in Chua's circuit was given in [7], where the existence of a Shilnikov-type homoclinic orbit is proved. A computer-assisted proof of chaotic behavior (more precisely of positive topological entropy) for the double-scroll attractor was presented in [8]. In [9], it was shown that there exist a trapping region for the double-scroll attractor. Rigorous study of the spiral attractor was carried out in [10]. The results listed above concern the circuit with a piece-wise linear characteristic of Chua's diode.

In this paper, we carry out rigorous analysis of Chua's circuit with a cubic nonlinearity [11], [12]. In Section II, we recall the definition of the circuit. In Section III, we analyze the behavior of the system in the periodic region. For each case we construct a trapping region enclosing the numerically observed attractor and carry out a complete study of the dynamics in the trapping region. In Section IV, we investigate the dynamics of the system for a parameter value in a period-3 window of the chaotic region. In Sections V and VI, we present results of the analysis of the spiral attractor and the double-scroll attractor. We find accurate lower bounds for the topological entropy of the associated return map and report results of the search for

Z. Galias is with the Department of Electrical Engineering, AGH University of Science and Technology, al. Mickiewicza 30, 30–059, Kraków, Poland, e-mail: galias@agh.edu.pl.

This work was supported in part by the AGH University of Science and Technology, grant no. 11.11.120.343.

Manuscript received Month ??, 2016; revised Month ??, 2016.

low-period orbits. We also discuss computational difficulties associated with the replacement of a piecewise linear function by a smooth nonlinearity.

An additional goal of this work is to show the importance of rigorous computations and present detailed examples how to use various interval arithmetic based tools to carry out a thorough analysis of dynamical behaviors of nonlinear systems. It is well known that due to rounding errors results obtained by numerical simulations of nonlinear systems may be unreliable, especially in case of chaotic systems [13]. When a trajectory of a dynamical system computed using standard numerical tools looks chaotic, we cannot be sure that the system is indeed chaotic. Computation of chaos detectors, like Lyapunov exponents, also does not provide conclusive answers. An observed trajectory may be a transient to a periodic steady-state or may be a result of numerical errors. Similarly, even if in simulations a steady state is periodic it does not mean that there are no chaotic trajectories in the system. An example of topological chaos existing in a period-3 window will be shown in Section IV.

II. CHUA'S CIRCUIT WITH A CUBIC NONLINEARITY

The dynamics of Chua's circuit with a cubic nonlinearity [11] shown in Fig. 1 is defined by

$$\begin{aligned} C_1 \dot{x}_1 &= (x_2 - x_1)/R - g(x_1), \\ C_2 \dot{x}_2 &= (x_1 - x_2)/R + x_3, \\ L \dot{x}_3 &= -x_2 - R_0 x_3, \end{aligned} \quad (1)$$

where $g(z) = g_1 z + g_2 z^3$. It is assumed that $g_1 < 0$ and all other parameters are positive. Electronic implementation of the cubic nonlinearity using two multipliers and one operational amplifier was described in [12].

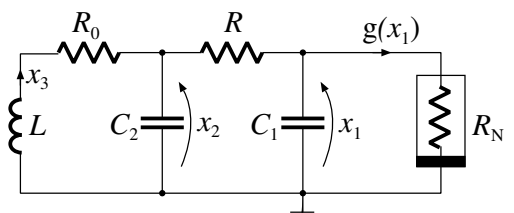


Fig. 1. Chua's circuit with a cubic nonlinearity.

We consider the system (1) with the following set of dimensionless parameters: $C_1 = 0.7$, $C_2 = 7.8$, $L = 1.891$, $R_0 = 0.01499$, $g_1 = -0.59$, $g_2 = 0.02$. Resistance $R \in [1.9, 2.2]$ is treated as a bifurcation parameter.

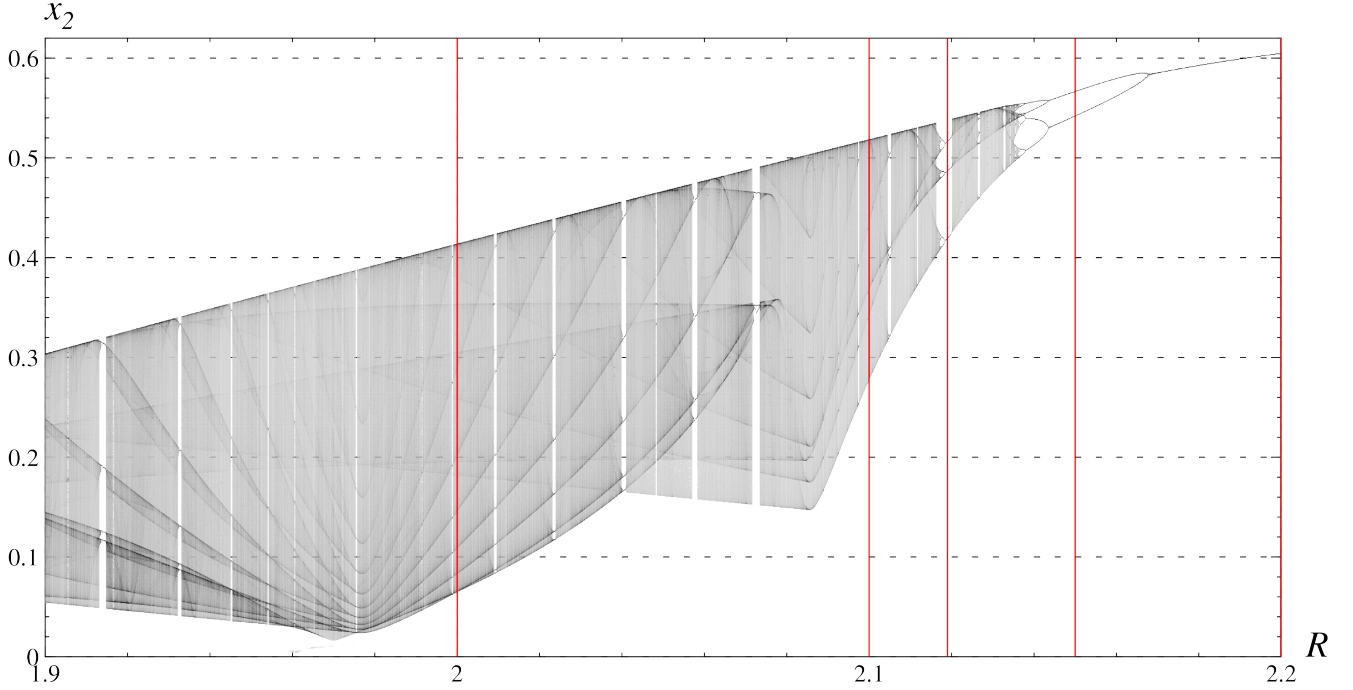


Fig. 2. Bifurcation diagram for Chua's circuit with cubic nonlinearity, $R \in [1.9, 2.2]$.

For $R > -g_1^{-1} - R_0 \approx 1.6799$, there exist three equilibria: the origin and a pair of symmetric equilibria

$$\pm x^* = \pm x_1^* (1, R_0(R_0+R)^{-1}, -(R_0+R)^{-1}), \quad (2)$$

where $x_1^* = \sqrt{-(g_1 + (R + R_0)^{-1})g_2^{-1}}$. In the considered parameter range $R \in [1.9, 2.2]$ the origin is unstable with one unstable direction and two stable directions. Equilibria $\pm x^*$ are stable for $R > \bar{R} \approx 2.222641$ and unstable for $R \leq \bar{R}$ with one stable direction and two unstable directions. When R is changed one can see a typical series of period doubling bifurcations leading to chaotic behavior. For $R > \bar{R}$ one observes convergence to one of the stable fixed points $\pm x^*$. They lose stability at $R = \bar{R}$ and two stable periodic orbits (one around each symmetric equilibrium) are born.

Fig. 2 shows a bifurcation diagram of the return map P_R defined by the half-plane $\Sigma_R = \{x = (x_1, x_2, x_3) \in \mathbb{R}^3 : x_1 = x_1^*, \dot{x}_1 \geq 0\}$, i.e. $P_R : \Sigma_R \mapsto \Sigma_R$ is defined as $P_R(x) = \varphi(\tau(x), x)$, where $\varphi(t, x)$ is the trajectory of (1) starting at x , and $\tau(x)$ is the return time after which the trajectory $\varphi(t, x)$ returns to Σ_R . Note that the half plane Σ_R is selected to contain the equilibrium x^* . In consequence, Σ_R and P_R depend on R . We have considered 6001 parameter values selected uniformly from the interval $R \in [1.9, 2.2]$. For each parameter value 10000 iterations are recorded after skipping 1000 iterations. The variable range $x_2 \in [0, 0.62]$ is divided into 1000 bins of equal length and bins are plotted using different shadows of gray according to the number of times a trajectory visits each bin.

In Fig. 2 one can see that for R close to 2.2 the trajectory of the return map is a single point, which corresponds to a periodic trajectory of (1) intersecting Σ_R once per period. When R is decreased this orbit loses stability and a stable

orbit with the period approximately two times longer is born. For smaller R one can see period-4 and period-8 windows. The sequence of period-doubling bifurcations leads to chaotic behavior in the form of a spiral attractor [11] (see also Fig. 7(a)). When R is further decreased two symmetric spiral attractors collide and a double-scroll attractor is observed (see Fig. 11(a)).

In the following sections, using interval arithmetic based tools we rigorously analyze dynamical behaviors of system (1) for several values of the bifurcation parameter R . Selected value are denoted in Fig. 2 as red solid lines. We will study the behavior of the system for two parameter values from the periodic region ($R = 2.2$, $R = 2.15$), and three parameter values from the chaotic region, including a parameter value from the largest period-3 window ($R = 2.119$), and parameter values for which a spiral attractor ($R = 2.1$) and a double-scroll attractor ($R = 2.0$) are observed.

III. PERIODIC REGION

Let us first consider the *periodic region*, which is observed roughly for $R > 2.1365$ (compare Fig. 2). In simulations, for $R = 2.2$ trajectories converge to a periodic orbit with one turn around x^* (see Fig. 3(a)). We will show that in this case for the corresponding return map there exist a trapping region which contains a single fixed point attracting all trajectories initiated in this trapping region.

Let us consider the return map P_1 defined by the half-plane $\Sigma_1 = \{x = (x_1, x_2, x_3) : x_1 = 2.63183, \dot{x}_1 \leq 0\}$. In the first step of analysis we find a possibly large trapping region for the map P_1 . A *trapping region* is a set in the domain of the map which is mapped into itself. The trapping region candidate, T ,

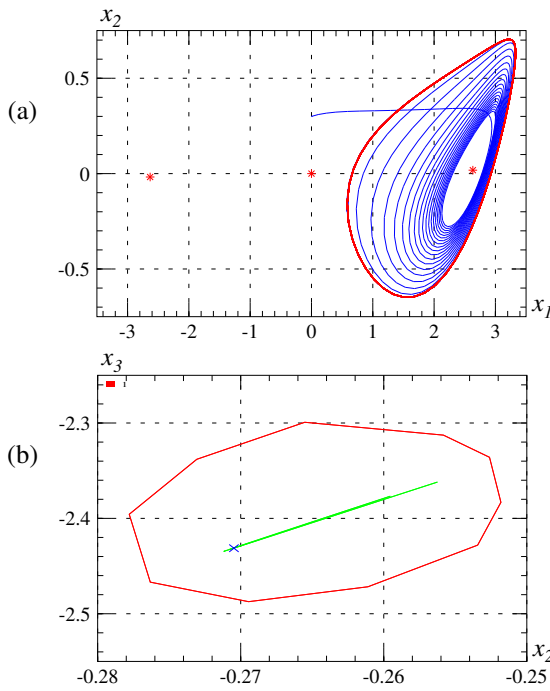


Fig. 3. (a) a trajectory (blue) of Chua's circuit converging to a stable periodic orbit (red) for $R = 2.2$; the three equilibria are plotted using star symbols, (b) The border of the trapping region T (red) for P_1 , its image computed non-rigorously (green), and the stable fixed point (\times) in T .

and its image, $P_1(T)$, computed non-rigorously, are shown in Fig. 3(b) in red and green, respectively.

In order to show that T is indeed a trapping region we have to prove that $P_1(T) \subset T$. This is done by covering T by boxes v_k (two-dimensional interval vectors), finding enclosures y_k of $P_1(v_k)$, and verifying conditions $y_k \subset T$. Evaluation of P_1 is done by rigorous integration of the vector field using the Lohner method [14]. Integration procedure was written in C++ using Profil/BIAS packages [15] for interval arithmetic computations. For details how to implement covering process using the generalized bisection method see [16], [17]. To speed up computations the border and the interior of T are handled separately. It is computationally more efficient to prove that the image of the border of T is enclosed in T and that the map is well defined on T than that the image of T is enclosed in T (compare [17]). The computer assisted proof that $P_1(T) \subset T$ required covering of the border and interior of T by 200 and 197 boxes, respectively.

All trajectories initiated in the trapping region stay there forever, and in consequence the trapping region must contain an attractor (or multiple attractors).

Non-transient dynamics takes place in the invariant part of the trapping region. We say that a point belongs to the *invariant part* $\text{Inv}(T)$ of a set T if there exist a trajectory entirely enclosed in T passing through this point. To find an enclosure of $\text{Inv}(T)$ we use the graph representation of the dynamics of the map [18], [16], [17]. First, the trapping region is covered by boxes of a given size and non-forbidden connections between the boxes are found. We say that the connection (v_i, v_j) between the boxes v_i and v_j is *forbidden*

if $P(v_i) \cap v_j = \emptyset$. Boxes which are not a starting point of any connection and boxes which are not an ending point of any connection are removed from the graph. This process is continued until no more boxes can be removed. To improve the approximation of the invariant part one may apply a finer division of the remaining boxes and redo the computations. This procedure has been applied to the set T . As a result we have found a set of 621 boxes of size $(1/6400) \times (1/6400)$ covering the invariant part. This set of boxes is enclosed in the interval vector w having area less than $5 \cdot 10^{-8}$. In the final step we prove that w contains a single fixed point attracting all trajectories starting in T . This is done by applying the interval Newton method [19] to prove the existence of a fixed point. Next, we verify that eigenvalues of the Jacobian matrix of the return map (evaluated on w) are enclosed in the unit circle which shows that the fixed point is stable. Lastly, we prove that the matrix norm of the Jacobian matrix is smaller than one. It follows from the Banach fixed-point theorem that all trajectories starting in w converge to this fixed point.

Thus, for $R = 2.2$ we have a complete description of the dynamics of the return map P_1 in T : all trajectories starting in T converge to the unique fixed point in T .

Let us now consider the case $R = 2.15$ for which, in simulations, trajectories converge to a periodic orbit with two turns around the equilibrium x^* (see Fig. 4(a)). This periodic orbit corresponds to a period-2 orbit of the return map.

We have proved that for $R = 2.15$ the polygon T shown in Fig. 4(b) is a trapping region for the return map P_2 defined by the plane $\Sigma_2 = \{x = (x_1, x_2, x_3) : x_1 = 2.53085, \dot{x}_1 \leq 0\}$. During the proof, the border and the interior T were covered by 691 and 192 boxes, respectively.

In this case, the invariant part is more complex than in the previous case and finding its accurate enclosure is more time-consuming. To uncover the underlying dynamical structure, we find an enclosure of the nonwandering part of trapping region. To eliminate parts containing non-recurrent dynamics, we remove boxes not belonging to any cycle in the graph (compare [17]). This procedure splits the invariant part into three connected components shown in Fig. 4(c). Using the interval Newton operator we prove that the two outer components contain a single period-2 orbit. Using the Banach fixed-point theorem we show that all trajectories with initial conditions belonging to these components are attracted to this period-2 orbit. We also prove that the middle component contains a single unstable fixed point. One can show that if a trajectory stays in a neighborhood of this fixed point forever, it has to converge to it. This can be done using a perturbation method to analyze dynamical behavior around a hyperbolic fixed point. It is clear that if a trajectory leaves a neighborhood of the fixed point, it will converge to the period-2 orbit.

In summary, we have shown that for $R = 2.15$ the dynamics of P_2 in the set T can be described as follows. There are two periodic solutions in T : the stable period-2 orbit and the unstable fixed point. Additionally, $\text{Inv}(T)$ contains the unstable manifold of the fixed point which connects it with the period-2 orbit. All trajectories starting in T converge to one of the two periodic solutions. Trajectories converging to the unstable fixed point will not be observed in simulations.

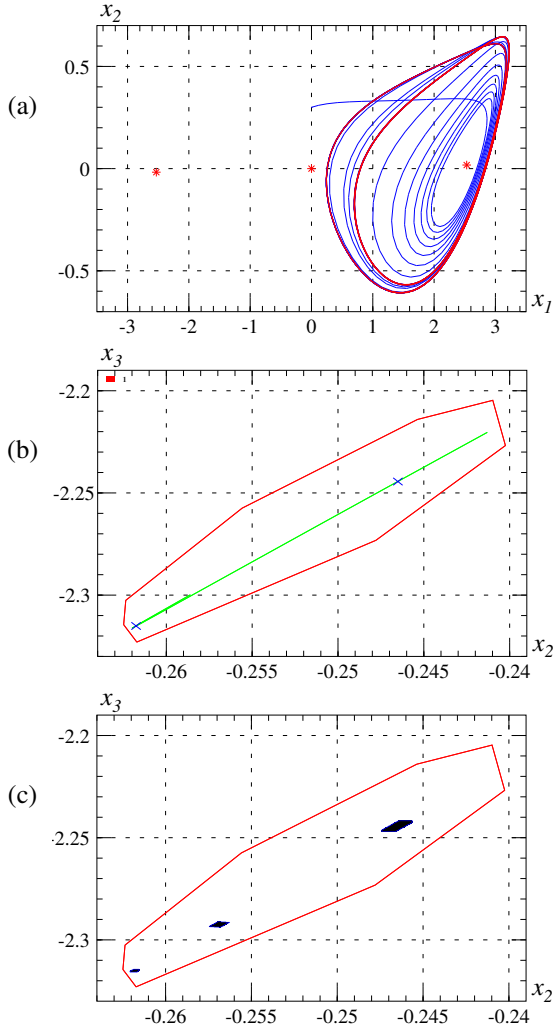


Fig. 4. (a) a trajectory (blue) of Chua's circuit converging to a stable periodic orbit (red) for $R = 2.15$, (b) the border of the trapping region T (red) for P_2 , its image computed non-rigorously (green), and the stable period-2 orbit (\times), (c) an enclosure of the non-wandering component of T (blue).

IV. PERIOD-3 WINDOW

After an infinite number of period-doubling bifurcations the system enters the chaotic region. For most parameter values belonging to the chaotic region one observes chaotic steady-state behavior. However, in the chaotic region there are also infinitely many periodic windows. The widest periodic window exists for R slightly smaller than 2.12 (compare Fig. 2). Let us consider the case $R = 2.119$ for which in simulations one observes convergence of trajectories to a periodic orbit with three turns around x^* (see Fig. 5(a)).

A trapping region candidate T for the return map P_3 defined by $\Sigma_3 = \{x = (x_1, x_2, x_3) : x_1 = 2.46368, \dot{x}_1 \leq 0\}$ is shown in Fig. 5(b). The candidate was constructed to enclose the period-3 stable orbit. The computer assisted proof that $P_3(T) \subset T$ required covering of the border and interior of T by 691 and 192 boxes, respectively.

Now, we show that the dynamics in the trapping region is *chaotic in the topological sense*, i.e. that the topological entropy of the return map is positive. There is a number

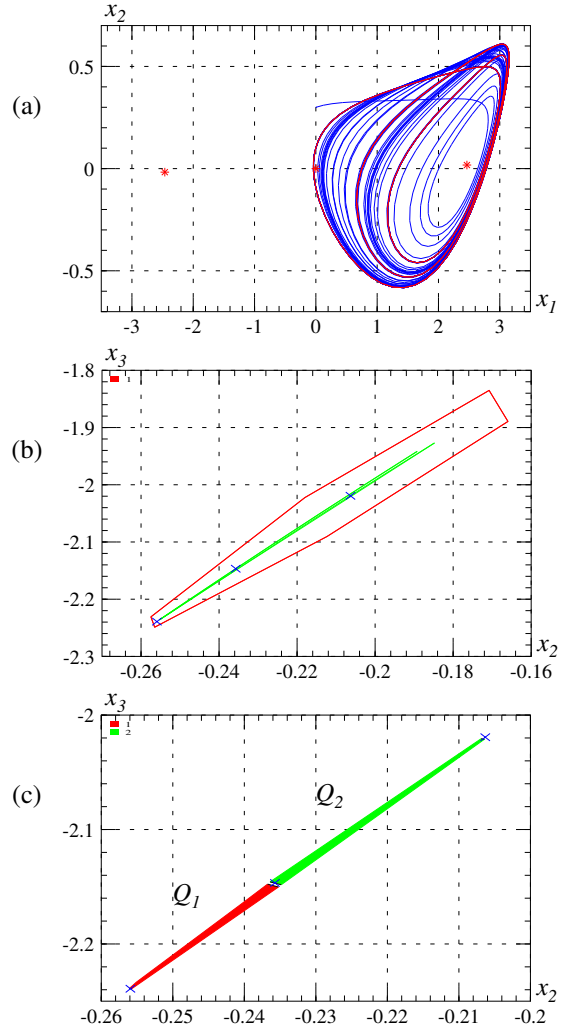


Fig. 5. (a) a trajectory (blue) of Chua's circuit converging to a stable periodic orbit (red) for $R = 2.119$, (b) the border of the trapping region T (red) for P_3 , its image computed non-rigorously (green), and stable period-3 orbit (\times), (c) sets Q_1 , Q_2 supporting symbolic dynamics for P_3 .

of methods which can be used to prove that a given map is topologically chaotic. One possible approach is via the Shilnikov's theorem, which states that if there exists a homoclinic loop of the saddle focus and some additional conditions hold then there are countably many saddle periodic orbits in a neighborhood of the homoclinic loop. Under these conditions there exists a topological Smale's horseshoe for an appropriately defined return map, and hence the topological entropy of the system is positive. However, the existence of a homoclinic loop can be usually proved only for some unknown parameter value belonging to a given interval. This approach has been used in [7] to prove that Chua's system with a piecewise linear nonlinearity is chaotic. In this work, we use the method based on proving the existence of covering relations [20], which will be described below. An approach based on extending Conley index techniques for constructing semi-conjugate symbolic dynamical systems has been presented in [21]. A semi-automatic method to locate complex covering relations based on a graph representation of the dynamics has

been proposed in [22]. A method to obtain rigorous lower bound for the topological entropy of planar diffeomorphisms based on the geometry of stable and unstable manifolds of hyperbolic periodic points has been presented in [23]. This method has an advantage that accurate estimates of the true entropy can be obtained. However, applying it in a rigorous way to return maps associated with continuous dynamical systems is difficult due to the necessity of finding rigorous enclosures of stable and unstable manifolds [24].

Let us briefly recall the method of covering relations (cf. [20], [8]). Let Q_1, Q_2, \dots, Q_p be pairwise disjoint sets. Each set Q_i is a topological rectangle with predefined vertical and horizontal edges. We say that $Q_i P$ -covers Q_j under a continuous map P if $P(Q_i)$ is enclosed in the interior of a topological stripe defined by horizontal edges of Q_j in such a way that images of vertical edges of Q_i lie geometrically on the opposite sides of Q_j . Examples are shown in Fig. 6. Covering relations are also referred to as *correctly aligned windows* [25].

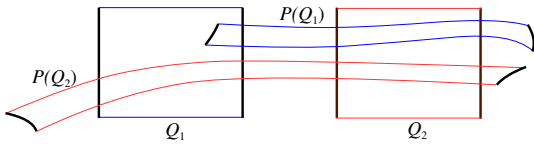


Fig. 6. Covering relations example: $Q_1 P$ -covers Q_2 , $Q_2 P$ -covers Q_1 and itself, vertical edges and their images are plotted in black.

From the existence of covering relations involving P one can obtain a lower bound for the topological entropy of P . The topological entropy $h(P)$ is not less than the logarithm of the dominant eigenvalue of the transition matrix $A \in \mathbb{R}^{p \times p}$ defined as $A_{ij} = 1$ if $Q_i P$ -covers Q_j , and $A_{ij} = 0$ otherwise (see [26]).

Candidate topological rectangles Q_1 and Q_2 found by a “trial-and-error” method are shown in Fig. 5(c). Their positions were adjusted so that nontrivial covering relations between Q_1 and Q_2 hold. It has been shown that $Q_1 P_3$ -covers both Q_2 and itself, while $Q_2 P_3$ -covers Q_1 . In the proof, the borders of Q_1 and Q_2 are covered by 5550 boxes, enclosures of their images are found, and it is verified that all conditions involving the three covering relations are satisfied. Covering relations between Q_1 and Q_2 correspond to the transition matrix

$$A_1 = \begin{pmatrix} 1 & 1 \\ 1 & 0 \end{pmatrix}, \quad (3)$$

which defines the golden mean shift on two symbols. The dominant eigenvalue of A_1 is $\lambda = 0.5 \cdot (\sqrt{5} + 1) \approx 1.618$. It follows that $h(P_3) \geq \log \lambda > 0.4812$.

Let us note that vertical edges of sets Q_1 and Q_2 are very close to positions of the stable period-3 orbit. This was unintentional; as mentioned before, the sets Q_1 and Q_2 were selected using the “trial-and-error” approach. However, this example shows that knowing positions of short periodic orbits may be helpful in finding good candidates for sets supporting complex symbolic dynamics (compare with [23]).

Simulations indicate that trajectories starting in T with probability one converge to the stable period-3 orbit. However,

from the existence of symbolic dynamics we also know that there are complex trajectories in T visiting sets Q_1 and Q_2 in any order allowed by the transition matrix A_1 . The number of fixed points of the p th iterate of the map is not less than the number of periodic sequences of length p admissible by the transition matrix. Since the number of such sequences for large p is close to λ^p it follows that the number of periodic orbits in T grows with the period p not slower than $1.618^p/p$.

Note that dynamical behaviors in this case are completely different from the ones existing for the periodic region. In the periodic region all trajectories converge to a periodic solution. For the period-3 window there are infinitely many periodic trajectories and there exist chaotic trajectories passing arbitrarily close to any periodic orbit. This example shows we have to be careful when we formulate conclusions based on results of standard numerical simulations. From the fact that in simulations we observe convergence of trajectories to a single periodic solution it does not follow that dynamical behaviors are simple—topological chaos may exist, like in this example.

V. ANALYSIS OF THE SPIRAL ATTRACTOR

Let us now consider the case $R = 2.1$ for which in simulations a spiral attractor is observed (see Fig. 7(a)).

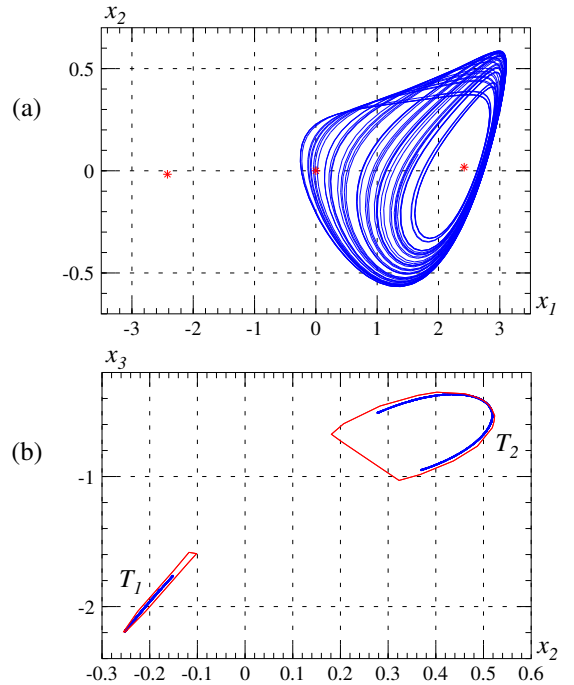


Fig. 7. (a) a trajectory of Chua’s circuit for $R = 2.1$, (b) a trajectory of the return map P_4 (blue) and the border of the trapping region $T_1 \cup T_2$ (red).

Let P_4 be a return map defined by the plane $\Sigma_4 = \{x = (x_1, x_2, x_3) : x_1 = 2.42058\}$. The trapping region $T = T_1 \cup T_2$ for the map P_4 is plotted in Fig. 7(b). T encloses the numerically observed attractor. The computer assisted proof that $P_4(T) \subset T$ requires covering of the border and the interior of T by 1251 and 454 boxes, respectively.

Now, we show that the dynamics in the trapping region is chaotic in the topological sense. Let us consider the return map P_5 defined by the half-plane $\Sigma_5 = \{x = (x_1, x_2, x_3) : x_1 =$

$2.42058, \dot{x}_1 < 0\}$. Candidate sets Q_1 and Q_2 are shown in Fig. 8(a). It has been shown that there are three covering relations between sets Q_1 and Q_2 corresponding to the golden mean shift. It follows that $h(P_5) > 0.4812$.

The sets Q_1 and Q_2 cover only a small part of the attractor. Therefore, one can expect that it should be possible to find more complex symbolic dynamics with larger entropy. A candidate consisting of five sets covering a larger part of the numerical trajectory is shown in Fig. 8(b). This candidate was found with the help of a semiautomatic method to locate complex symbolic dynamics [22]. It was proved that the transition matrix is

$$A_2 = \begin{array}{|c|c|c|c|c|} \hline & \text{1} & \text{2} & \text{3} & \text{4} \\ \hline \text{1} & 0 & 1 & 0 & 0 \\ \hline \text{2} & 1 & 0 & 1 & 0 \\ \hline \text{3} & 0 & 0 & 0 & 1 \\ \hline \text{4} & 0 & 0 & 1 & 0 \\ \hline \end{array}, \quad (4)$$

where zeros and ones are denoted as white and black squares, respectively. Since the dominant eigenvalue of A_2 is $\lambda \approx 1.7407$ the lower bound is improved to $h(P_5) > 0.5542$.

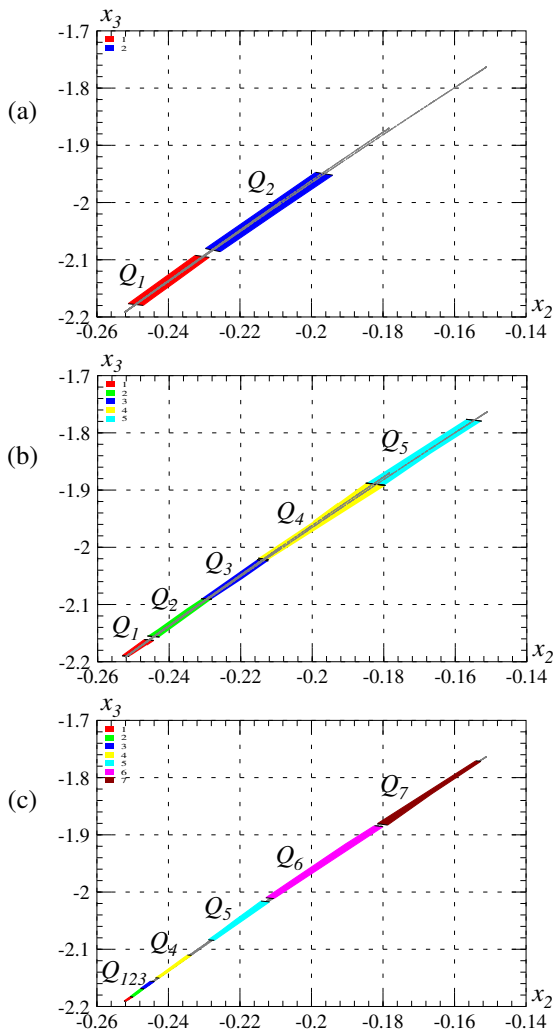


Fig. 8. Sets supporting symbolic dynamics for P_5 with the transition matrix A_1 (a), A_2 (b), and A_3 (c); vertical edges are plotted in black, a trajectory is plotted in gray.

One can still improve the estimate of the topological entropy $h(P)$ of P_5 by introducing a finer representation of the dynamics in

the lower-left corner of the attractor. Indeed, it has been proved that there are 12 covering relations between sets Q_1, Q_2, \dots, Q_7 shown in Fig. 8(c). These covering relations correspond to the transition matrix

$$A_3 = \begin{array}{|c|c|c|c|c|} \hline & \text{1} & \text{2} & \text{3} & \text{4} \\ \hline \text{1} & 0 & 1 & 0 & 0 \\ \hline \text{2} & 1 & 0 & 1 & 0 \\ \hline \text{3} & 0 & 0 & 0 & 1 \\ \hline \text{4} & 0 & 0 & 1 & 0 \\ \hline \end{array}. \quad (5)$$

The dominant eigenvalue of A_3 is $\lambda > 1.8138$ and hence

$$h(P_5) > \log 1.8138 > 0.5954. \quad (6)$$

To evaluate the bounds obtained, let us now estimate what is the true topological entropy of P_5 . The estimate is based on the number of short periodic orbits. Short periodic orbits can be found using the monitoring trajectory approach. In this method one selects a small positive number δ and searches a trajectory $(x^{(i)})_{i=1}^N$ for δ -pseudo periodic orbits, i.e. pieces of the trajectory such that the distance between the $x^{(i)}$ and $x^{(i+p)}$ is smaller than δ . In a neighborhood of a δ -pseudo periodic orbit there may exist a true periodic orbit. Let us assume that $(\bar{x}^{(i)}, \bar{x}^{(i+1)}, \dots, \bar{x}^{(i+p-1)})$ is a δ -pseudo periodic orbit of length p . An approximate position of the periodic orbit can be found applying the Newton method to locate zeros of the map $F: \mathbb{R}^p \mapsto \mathbb{R}^p$ defined by

$$[F(z)]_k = x^{((k+1) \bmod p)} - P(x^{(k)}) \text{ for } 0 \leq k < p,$$

where $z = (x^{(0)}, x^{(1)}, \dots, x^{(p-1)})$ with the initial condition $z^{(0)} = (\bar{x}^{(i)}, \bar{x}^{(i+1)}, \dots, \bar{x}^{(i+p-1)})$. The existence of the periodic orbit can be verified using the interval Newton method applied to an interval vector containing the approximate position. Once the existence is proved the interval vector containing the orbit is recorded. This information is used in further computations to verify whether periodic orbits located in the search process were not already found before. Using this method we have found 42995 periodic orbits with periods $p \leq 20$. It has been verified that all these orbits are unstable. The twelve shortest periodic orbits are plotted in Fig. 9.

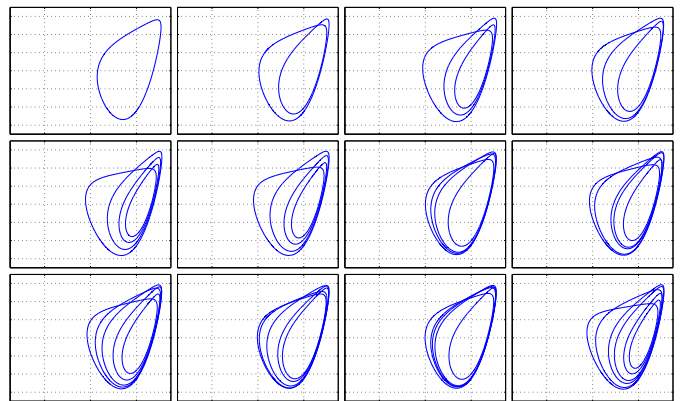


Fig. 9. Shortest unstable periodic orbits for Chua's circuit embedded in the spiral attractor; axes range: $(x_1, x_2) \in [-3.5, 3.5] \times [-0.7, 0.7]$.

Under certain assumptions the topological entropy $h(P)$ of the map P can be computed as

$$h(P) = \lim_{p \rightarrow \infty} \frac{1}{p} \log N_p, \quad (7)$$

where N_p is the number of fixed points of P^p (compare [26]). The expression $h_p = \frac{1}{p} \log N_p$ is often used as an estimate of the topological entropy, even when the assumptions under which (7) holds are not satisfied.

The numbers N_p of fixed points of P_5^p are plotted in Fig. 10(a) as a solid blue curve. For comparison we also plot the number of fixed points of P_5^p obtained from the existence of symbolic dynamics, which has been proved before. The number N_p of fixed points of P_5^p corresponding to the existence of the symbolic dynamics with the transition matrix A can be computed as the trace (the sum of diagonal entries) of the matrix A^p (see [27]). The results obtained for transition matrices A_1 , A_2 and A_3 are plotted in Fig. 10(a) as red, green and magenta dashed lines, respectively. Note that with the transition matrix A_3 we capture most of the periodic orbits found in the trajectory monitoring approach.

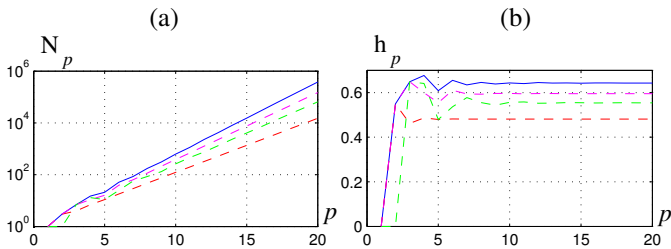


Fig. 10. (a) the number N_p of fixed points of P_5^p found using trajectory monitoring approach (blue solid line) and corresponding to symbolic dynamics with transition matrices A_1 , A_2 , and A_3 (red, green and magenta dashed lines), (b) estimates h_p of the topological entropy P_5 of based on the number of short orbits.

Estimates h_p obtained from the number of found periodic orbits are shown in Fig. 10(b) as a solid blue curve. The results for $p \in [10, 20]$ oscillate in the interval $[0.640, 0.645]$, which indicates that the true topological entropy belongs to this interval. Note that the rigorous lower bound (6) is close to this estimate.

VI. ANALYSIS OF THE DOUBLE-SCROLL ATTRACTOR

Let us now consider the case $R = 2.0$, where in simulations one observes a double-scroll attractor (compare Fig. 11(a)). Since trajectories scroll around both fixed points, it is more convenient to use a return map defined by two planes. We will use the return map P_{67} defined by the union of the planes $\Sigma_{6,7} = \{x = (x_1, x_2, x_3) : x_1 = \pm 2.1647\}$.

An example trajectory of the return map P_{67} is shown in Fig. 11(b). The plot is composed of four parts R_1 , R_2 , R_3 , and R_4 . The parts R_1 and R_2 correspond to intersections with Σ_6 while R_3 and R_4 correspond to intersections with Σ_7 . Points for which the previous iteration and the next iteration belong to the same plane as the current one are plotted in blue. Points whose image (preimage) belong to the different plane then the current one are plotted in red (black). Points in R_2 go to R_1 . Blue points in R_1 go to the blue spiral in R_2 , while red points in R_1 go to the black spiral in R_4 . One can see that the dynamics of the double-scroll attractor is richer than for the spiral attractor, where the red and black parts are missing and the blue spiral is not fully developed (cf. Fig. 7(b)).

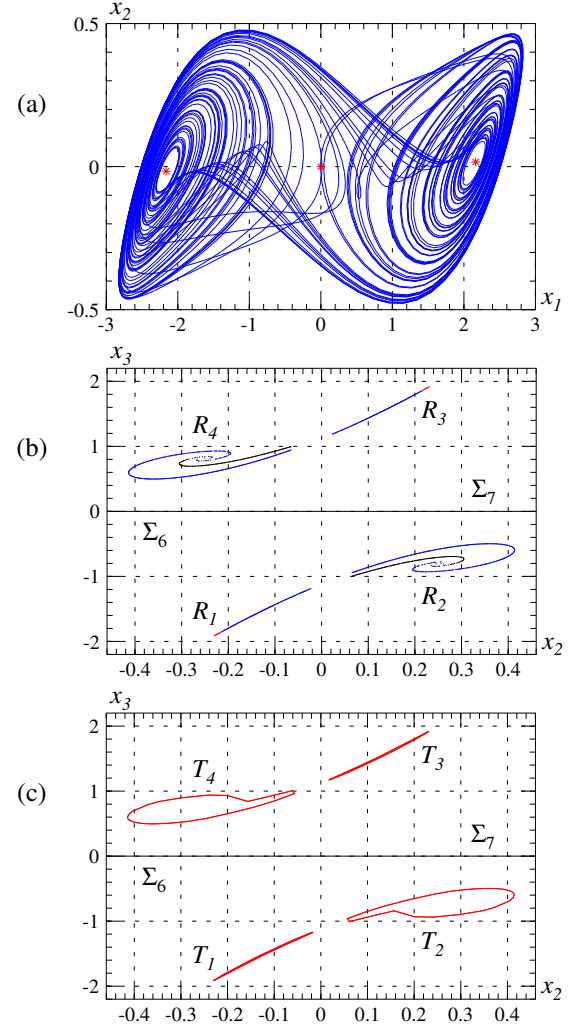


Fig. 11. (a) a trajectory of Chua's circuit for $R = 2.0$, (b) intersection of a trajectory with the planes Σ_6 (the lower half of the plot) and Σ_7 (the upper part of the plot), (c) border of the trapping region candidate $T = T_1 \cup T_2 \cup T_3 \cup T_4$ for the map P_{67} , $T_1 \cup T_2 \subset \Sigma_6$, $T_3 \cup T_4 \subset \Sigma_7$.

A candidate T for a trapping region shown in Fig. 11(c) is the union of polygons T_k , each enclosing one part of numerically observed trajectories. Polygons $T_3, T_4 \subset \Sigma_7$ are symmetric to $T_1, T_2 \subset \Sigma_6$. Polygons T_1 and T_2 were constructed in such a way that for test points $v_k \in T_1 \cup T_2$ the conditions $P_{67}(v_k) \in T$ are verified in non-rigorous computations. These conditions, if satisfied, indicate that T is a good candidate for a trapping region.

Applying the procedure to prove that T is a trapping region results in a covering of the border of $T_1 \cup T_2$ composed of 6320 boxes v_k . For 6288 boxes the condition $P_{67}(v_k) \subset T$ holds. However, the procedure fails for 32 boxes lying close to the region in T_1 where P_{67} is discontinuous. The discontinuity is a consequence of the fact that the double scroll attractor contains the origin, an unstable equilibrium. There are trajectories starting in T_1 which pass arbitrarily close to the origin. These trajectories are repelled from the origin along one of the two directions of its one-dimensional unstable manifold and reach either T_2 or T_4 (cf. Fig. 11(b)). It follows that it is not possible

to prove that $P_{67}(T_1) \subset T$ using standard rigorous integration methods. Rigorous evaluation of the return map for boxes containing discontinuity points requires developing procedures handling trajectories passing arbitrarily close to an equilibrium with infinitely large return times. The case of piecewise linear systems was considered in [9], where the existence of a trapping region for the double-scroll attractor was proved. For general nonlinear systems the unstable manifold is not a straight line and a different approach has to be used (see [28]). This problem is left for future study.

To investigate the existence of complex symbolic dynamics we consider the map P_{89} defined by the union of half-planes $\Sigma_{8,9} = \{x = (x_1, x_2, x_3) : x_1 = \pm 2.1647, \pm \dot{x}_1 < 0\}$, i.e. we limit ourselves to the polygons T_1 and T_3 .

First, we will consider the case of covering relation between sets belonging to a single plane. Candidate rectangles Q_1, Q_2 and Q_3 are shown in Fig. 12(a). Due to very strongly repelling in Q_1 the set $Q_1 P_{89}$ -covers all three sets. The set $Q_2 P_{89}$ -covers Q_1 and Q_3 . P_{89} -covers Q_2 . The existence of these five covering relations has been proved rigorously. During the proof borders of sets Q_1, Q_2 and Q_3 were covered by 761 boxes. The corresponding transition matrix

$$A_4 = \begin{matrix} & \begin{smallmatrix} \textcolor{red}{\blacksquare} & \textcolor{blue}{\blacksquare} \\ \textcolor{blue}{\blacksquare} & \textcolor{red}{\blacksquare} \end{smallmatrix} \end{matrix} \quad (8)$$

has the dominant eigenvalue $\lambda > 1.8393$ and hence: $h(P_{89}) > \log 1.8393 > 0.6093$.

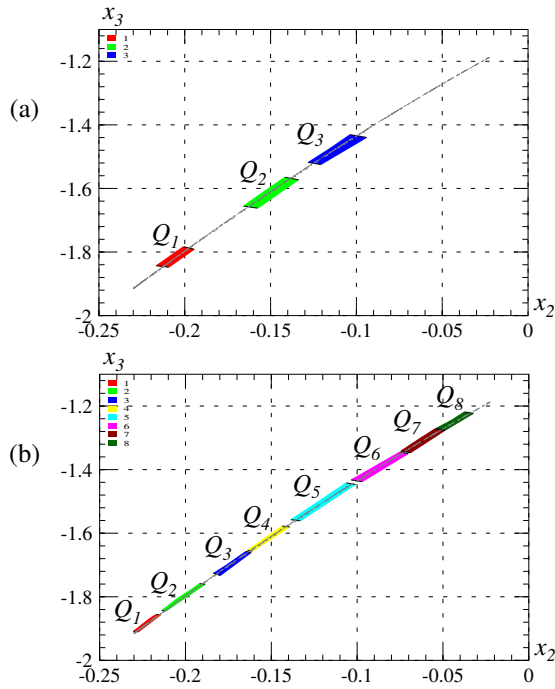


Fig. 12. Sets supporting symbolic dynamics for P_{89} with the transition matrix A_4 (a), and A_5 (b).

Let us note that although the symbolic dynamics with the transition matrix A_4 involves a single scroll only, the corresponding bound is better than the best bound (6) obtained for the spiral attractor.

To improve lower bounds we will use covering relations involving both scrolls. Candidate sets $Q_1, Q_2, \dots, Q_8 \subset \Sigma_8$

are shown in Fig. 12(b). These sets together with their symmetric copies $Q'_1, Q'_2, \dots, Q'_8 \subset \Sigma_9$ support complex symbolic dynamics. The set Q_1 is mapped by P_{89} into T_3 while the remaining sets are mapped into T_1 . We have proved the existence of 34 covering relations between sets Q_k and Q'_k which can be represented as the following transition matrix

$$A_5 = \begin{matrix} & \begin{smallmatrix} \textcolor{red}{\blacksquare} & \textcolor{blue}{\blacksquare} & \textcolor{magenta}{\blacksquare} & \textcolor{cyan}{\blacksquare} & \textcolor{yellow}{\blacksquare} & \textcolor{orange}{\blacksquare} & \textcolor{purple}{\blacksquare} \\ \textcolor{red}{\blacksquare} & \textcolor{black}{\blacksquare} & \textcolor{black}{\blacksquare} & \textcolor{black}{\blacksquare} & \textcolor{black}{\blacksquare} & \textcolor{black}{\blacksquare} & \textcolor{black}{\blacksquare} \\ \textcolor{blue}{\blacksquare} & \textcolor{black}{\blacksquare} & \textcolor{black}{\blacksquare} & \textcolor{black}{\blacksquare} & \textcolor{black}{\blacksquare} & \textcolor{black}{\blacksquare} & \textcolor{black}{\blacksquare} \\ \textcolor{magenta}{\blacksquare} & \textcolor{black}{\blacksquare} & \textcolor{black}{\blacksquare} & \textcolor{black}{\blacksquare} & \textcolor{black}{\blacksquare} & \textcolor{black}{\blacksquare} & \textcolor{black}{\blacksquare} \\ \textcolor{cyan}{\blacksquare} & \textcolor{black}{\blacksquare} & \textcolor{black}{\blacksquare} & \textcolor{black}{\blacksquare} & \textcolor{black}{\blacksquare} & \textcolor{black}{\blacksquare} & \textcolor{black}{\blacksquare} \\ \textcolor{yellow}{\blacksquare} & \textcolor{black}{\blacksquare} & \textcolor{black}{\blacksquare} & \textcolor{black}{\blacksquare} & \textcolor{black}{\blacksquare} & \textcolor{black}{\blacksquare} & \textcolor{black}{\blacksquare} \\ \textcolor{orange}{\blacksquare} & \textcolor{black}{\blacksquare} & \textcolor{black}{\blacksquare} & \textcolor{black}{\blacksquare} & \textcolor{black}{\blacksquare} & \textcolor{black}{\blacksquare} & \textcolor{black}{\blacksquare} \\ \textcolor{purple}{\blacksquare} & \textcolor{black}{\blacksquare} & \textcolor{black}{\blacksquare} & \textcolor{black}{\blacksquare} & \textcolor{black}{\blacksquare} & \textcolor{black}{\blacksquare} & \textcolor{black}{\blacksquare} \end{smallmatrix} \end{matrix}. \quad (9)$$

The dominant eigenvalue of the transition matrix is larger than 2.2774 and hence

$$h(P_{89}) > \log 2.2774 > 0.823. \quad (10)$$

This shows that, as expected, the dynamics of the double scroll attractor is richer than the dynamics of the spiral attractor.

We have used the monitoring trajectory approach to find short periodic orbits embedded in the double scroll attractor. The search procedure returned 602191 periodic orbits with periods $p \leq 20$. This is significantly more than for the spiral attractor with 42995 periodic orbits found (85990 for two coexisting spiral attractors). Shortest periodic orbits are plotted in Fig. 13. Two of these orbits are self-symmetric with respect to the origin. The remaining are 10 pairs of asymmetric orbits.

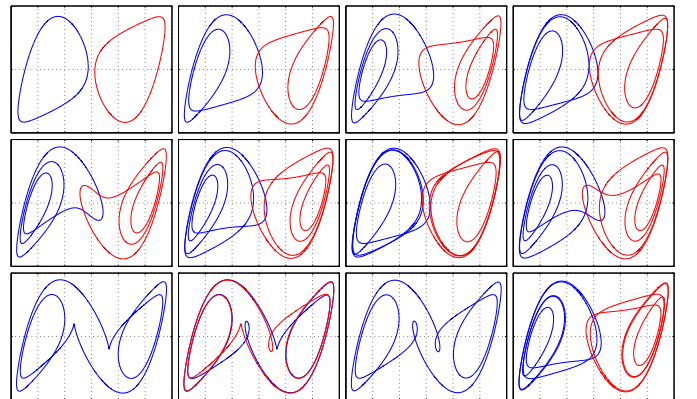


Fig. 13. Shortest periodic orbits for Chua's circuit embedded in the double scroll attractor; axes range: $(x_1, x_2) \in [-3, 3] \times [-0.5, 0.5]$.

Fig. 14(a) shows the number N_p of fixed points of P_{89}^p versus the period p . The results obtained from the monitoring trajectory technique are plotted as a blue solid line. The results corresponding to the existence of symbolic dynamics with the transition matrices A_4 and A_5 are plotted as red and green dashed lines, respectively. Let us note that for $p \geq 17$, the number of periodic orbits found using the monitoring trajectory approach is lower than the number of periodic orbits corresponding to the transition matrix A_5 . This is due to the amount of existing orbits—very long computation time is needed to pass sufficiently close to all short periodic orbits to guarantee the convergence of the Newton method. Fig. 14(a)

shows estimates h_p of the entropy of the return map P_{89} based on N_p . The estimates reach $h_p \approx 0.964$ for $p \in \{8, 9, 10\}$ and drop fast for $p \geq 11$. It follows that for the double-scroll attractors one cannot draw conclusions about the true value of the topological entropy based on the number of periodic orbits found using the monitoring trajectory approach.

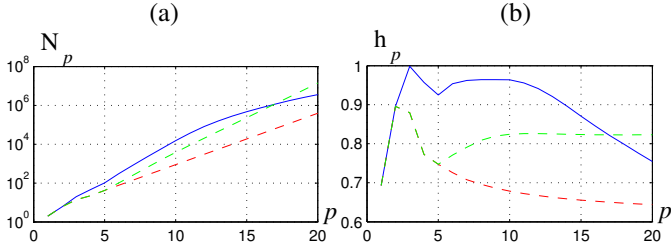


Fig. 14. (a) the number N_p of fixed points of P_{89}^p , (b) estimates h_p of the topological entropy of P_{89} based on the number of short orbits.

VII. CONCLUSIONS

Dynamics of Chua's circuit with a cubic nonlinearity has been analyzed for several parameter values in the periodic and chaotic regions. For two parameters values in the periodic region a complete characterization of dynamical phenomena has been carried out. In all cases apart from the double-scroll attractor, trapping regions for the corresponding return map have been constructed. It was explained why it is impossible to prove the existence of a trapping region in the case of the double-scroll attractor using available rigorous integration methods. This problem is left for future study. Accurate lower bounds of the topological entropy have been found and it has been proved that Chua's circuit is chaotic in the topological sense for the cases of the stable period-3 orbit, the spiral attractor and the double scroll attractor. The existence of many (hundreds of thousands) unstable periodic orbits embedded in chaotic attractors have been proved using the combination of the interval Newton operator and the monitoring trajectory approach. The results have been used to estimate the true value of topological entropy.

REFERENCES

- [1] L. O. Chua, M. Komuro, and T. Matsumoto, "The double scroll family," *IEEE Trans. Circuits Syst.*, vol. 33, pp. 1037–1118, Nov. 1986.
- [2] T. Matsumoto, L. O. Chua, and M. Komuro, "The double scroll," *IEEE Trans. Circuits Syst.*, vol. 32, no. 8, pp. 798–817, Aug. 1985.
- [3] L. O. Chua and G. N. Lin, "Canonical realisation of Chua's circuit family," *IEEE Trans. Circuits Syst.*, vol. 37, no. 7, pp. 885–902, July 1990.
- [4] M. Komuro, R. Tokunaga, T. Matsumoto, L. O. Chua, and A. Hotta, "Global bifurcation analysis of the double scroll circuit," *Int. J. Bifurcation Chaos*, vol. 1, no. 1, pp. 139–182, 1991.
- [5] L. O. Chua, "Global unfolding of Chua's circuit," *IEICE Trans. Fundam.*, vol. 76, no. 5, pp. 704–734, 1993.
- [6] R. N. Madan, *Chua's Circuit: A Paradigm for Chaos*. Singapore: World Scientific, 1993.
- [7] T. Matsumoto, L. O. Chua, and K. Ayaki, "Reality of chaos in the double scroll circuit: A computer-assisted proof," *IEEE Trans. Circuits Syst.*, vol. 35, no. 7, pp. 909–925, July 1988.
- [8] Z. Galias, "Positive topological entropy of Chua's circuit: A computer assisted proof," *Int. J. Bifurcation Chaos*, vol. 7, no. 2, pp. 331–349, 1997.
- [9] ———, "Trapping region for the double scroll attractor," in *Proc. IEEE Int. Symp. Circuits Syst. (ISCAS)*, May 2012, pp. 401–404.
- [10] ———, "Rigorous study of the Chua's circuit spiral attractor," *IEEE Trans. Circuits Syst. I*, vol. 59, no. 10, pp. 2374–2382, 2012.
- [11] A. Khibnik, D. Roose, and L. O. Chua, "On periodic and homoclinic bifurcations in Chua's circuits with a smooth nonlinearity," *Int. J. Bifurcation Chaos*, vol. 3, no. 2, pp. 363–384, 1993.
- [12] G. Zhong, "Implementation of Chua's circuit with a cubic nonlinearity," *IEEE Trans. Circuits Syst. I*, vol. 41, no. 12, pp. 934–941, 1994.
- [13] R. Lozi, "Can we trust in numerical computations of chaotic solutions of dynamical systems?" in *Topology and Dynamics of Chaos*, C. Letellier and R. Gilmore, Eds. World Scientific, 2013, vol. 84, pp. 29–64.
- [14] R. J. Lohner, "Computation of guaranteed enclosures for the solutions of ordinary initial and boundary value problems," in *Computational Ordinary Differential Equations*, J. Cash and I. Gladwell, Eds. Oxford: Clarendon Press, 1992.
- [15] O. Knüppel, "PROFIL/BIAS—a fast interval library," *Computing*, vol. 53, no. 3–4, pp. 277–287, 1994.
- [16] M. Dellnitz and A. Hohmann, "A subdivision algorithm for the computation of unstable manifolds and global attractors," *Numerische Mathematik*, vol. 75, pp. 293–317, 1997.
- [17] Z. Galias, "The dangers of rounding errors for simulations and analysis of nonlinear circuits and systems — and how to avoid them," *IEEE Circuits Syst. Mag.*, vol. 13, no. 3, pp. 35–52, 2013.
- [18] M. Dellnitz, A. Hohmann, O. Junge, and M. Rumpf, "Exploring invariant sets and invariant measures," *Chaos: Interdiscipl. J. Nonlinear Sci.*, vol. 7, no. 2, pp. 221–228, 1997.
- [19] A. Neumaier, *Interval Methods for Systems of Equations*. Cambridge, UK: Cambridge University Press, 1990.
- [20] P. Zgliczyński, "Computer assisted proof of chaos in the Rössler equations and in the Hénon map," *Nonlinearity*, vol. 10, no. 1, pp. 243–252, 1997.
- [21] S. Day, R. Frongillo, and R. Trevino, "Algorithms for rigorous entropy bounds and symbolic dynamics," *SIAM J. Applied Dynamical Systems*, vol. 7, no. 4, pp. 1477–1506, 2008.
- [22] Z. Galias, "Automated search for complex symbolic dynamics with applications in the analysis of a simple memristor circuit," *Int. J. Bifurcation Chaos*, vol. 24, no. 7, p. 1450104 (11 pages), 2014.
- [23] S. Newhouse, M. Berz, J. Grote, and K. Makino, "On the estimation of topological entropy on surfaces," *Contemp. Math.*, vol. 469, pp. 243–270, 2008.
- [24] M. Capiński and P. Zgliczyński, "Geometric proof for normally hyperbolic invariant manifolds," *Journal of Differential Equations*, vol. 259, no. 11, pp. 6215–6286, 2015.
- [25] P. Zgliczyński and M. Gidea, "Covering relations for multidimensional dynamical systems I," *J. Differ. Equ.*, vol. 27, no. 1, pp. 32–58, 2004.
- [26] C. Robinson, *Dynamical Systems: Stability, Symbolic Dynamics, and Chaos*. Boca Raton, FL, USA: CRC Press, 1995.
- [27] R. Devaney, *An Introduction to Chaotic Dynamical Systems*. Boulder, CO, USA: Westview Press, 2003.
- [28] W. Tucker, "A rigorous ODE solver and Smale's 14th problem," *Found. Comput. Math.*, vol. 2, no. 1, pp. 53–117, 2002.



Zbigniew Galias received the M.Sc. degree in Electronics from the AGH University of Science and Technology, Kraków, Poland in 1990, the M.Sc. degree in Mathematics from the Jagiellonian University, Kraków in 1992, and the Ph.D. degree and the senior doctorate degree in Electrical Engineering from the AGH University of Science and Technology, Kraków in 1996 and 2004, respectively. In 2015, he was conferred the title of Professor by the President of the Republic of Poland.

Since 2005, he is a Professor of Electrical Engineering at the AGH University of Science and Technology, Kraków. He has held visiting research positions at the Technical University Munich, the University of California at Berkeley, the University of California at San Diego, and the RMIT University, Melbourne. He was awarded the Polish Research Foundation scholarship in 1994, received the Polish Prime Minister award for the Ph.D. thesis in 1997, and was awarded the Fulbright fellowship in 1999. He served/is serving as an Associate Editor of IEEE Transaction on Circuits and Systems I and II, IEEE Circuits and Systems Magazine, and International Journal of Bifurcation and Chaos.